ACS APPLIED MATERIALS & INTERFACES

Research Article

www.acsami.org

Reduced Graphene Oxide for Catalytic Oxidation of Aqueous Organic Pollutants

Hongqi Sun,* Shizhen Liu, Guanliang Zhou, Ha Ming Ang, Moses O Tadé, and Shaobin Wang*

Department of Chemical Engineering and CRC for Contamination Assessment and Remediation of the Environment (CRC-CARE), Curtin University, GPO Box U1987, WA 6845, Australia

Supporting Information

ABSTRACT: We discovered that chemically reduced graphene oxide, with an I_D/I_G >1.4 (defective to graphite) can effectively activate peroxymonosulfate (PMS) to produce active sulfate radicals. The produced sulfate radicals ($SO_4^{\bullet-}$) are powerful oxidizing species with a high oxidative potential (2.5−3.1 vs 2.7 V of hydroxyl radicals), and can effectively decompose various aqueous contaminants. Graphene demonstrated a higher activity than several carbon allotropes, such as activated carbon (AC), graphite powder (GP), graphene oxide (GO), and multiwall carbon nanotube (MWCNT). Kinetic study of graphene catalyzed activation of PMS was carried out. It was shown that graphene catalysis is superior to that on transition metal oxide (Co_3O_4) in degradation of phenol, 2,4-dichlorophenol (DCP) and a dye (methylene blue, MB) in water, therefore providing a novel strategy for environmental remediation.

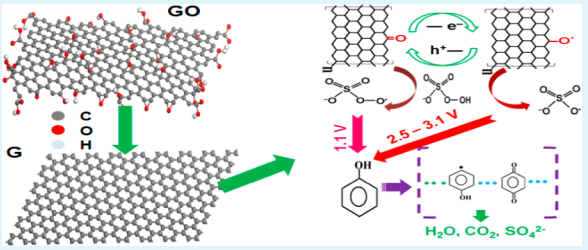

KEYWORDS: *graphene, peroxymonosulfate, oxidation, aqueous organics, phenol, sulfate radicals*

1. INTRODUCTION

Catalysis has dramatically prompted the success in environmental remediation for removal of toxic gases, NO_x, SO_x, VOCs (volatile organic compounds), and aqueous organic pollutants.[1−6] Current catalytic processes, which facilitate the efficient decontaminations, heavily depend on metal active sites. As a result, expensive noble metals and toxic transition metals (or oxides) have been widely consumed.[7−9]

Compared to gas-phase reactions, the negative effects derived from the utilization of transition metals become much worse in liquid phase. Secondary contaminations, such as leached metal ions, can be a direct risk to water body. In recent studies, sulfates radicals demonstrated a superiority to hydroxyl radicals owing to a high oxidative potential (2.5−3.1 vs 2.7 V of hydroxyl radicals), flexible capacity to a large range pH, and free of coagulation.[10] Homogeneous Co(II)/peroxymonosulfate (PMS) system was proven to be highly efficient for oxidation of various organic contaminants.[11−13] The barrier of such a process is the requirement of a cobalt-based catalyst for activation of PMS, as cobalt ion is recognized as a priority pollutant to water and causes many health issues. Heterogeneous catalysis using cobalt oxide[14] or supported cobalt oxide[5,10,15,16] has been investigated, yet cobalt leaching stubbornly occurs. Therefore, a metal-free catalyst that features cost-effective and environmental benign would be highly in demand in view of green and sustainable development.[17]

Recently, emerging nanocarbons as catalysts showed promising merits in nontoxicity, large surface area, high activity/selectivity, and good stability.[18−20] Nanocarbons such as carbon nanotubes (CNTs),[21−23] nanodiamond,[24] fullerene,[25] and graphene oxide (GO)[19,20,26] have demonstrated higher performances in synthetic reactions than bulk carbon allotropes. These catalytic reactions were carried out in gas-phase and ketonic C═O groups formed at graphene zigzag edges were suggested to be the catalytic active sites.

In liquid-phase catalysis, only few examples have been reported using nanocarbons, such as GO,[27] GO/CNT hybrid,[28] and nanodiamond[29] as a photocatalyst. For water purification, the main application of graphene (oxide) is adsorption of dyes[30,31] or heavy metal,[32] while the efficiency of graphene-based materials in catalysis is rather low.[33] In a previous study, we observed that activated carbon showed a notable activity in PMS activation.[5] Exploring a nanocarbon as a novel catalyst without secondary contamination for catalytic oxidation of aqueous organics would be of interests for a promising remediation of water.

Herein, for the first time, we demonstrate that a nanocarbon, reduced graphene oxide, can effectively activate PMS for producing sulfate radicals. The activity of graphene was higher than graphite powder (GP), activated carbon (AC), carbon nanotube (CNT), and graphene oxide (GO). Moreover, graphene was able to more efficiently degrade phenol, 2,4-dichlorophenol (DCP) and methylene blue (MB) than a typical cobalt catalyst, Co_3O_4 nanoparticles.

2. EXPERIMENTAL SECTION

Catalyst Preparation. Graphene oxide (GO) was prepared by a modified Hummers' method.[34] Graphite powder (GP) was oxidized by

Received: July 19, 2012
Accepted: September 11, 2012
Published: September 11, 2012

   dx.doi.org/10.1021/am301372d | ACS Appl. Mater. Interfaces 2012, 4, 5466−5471

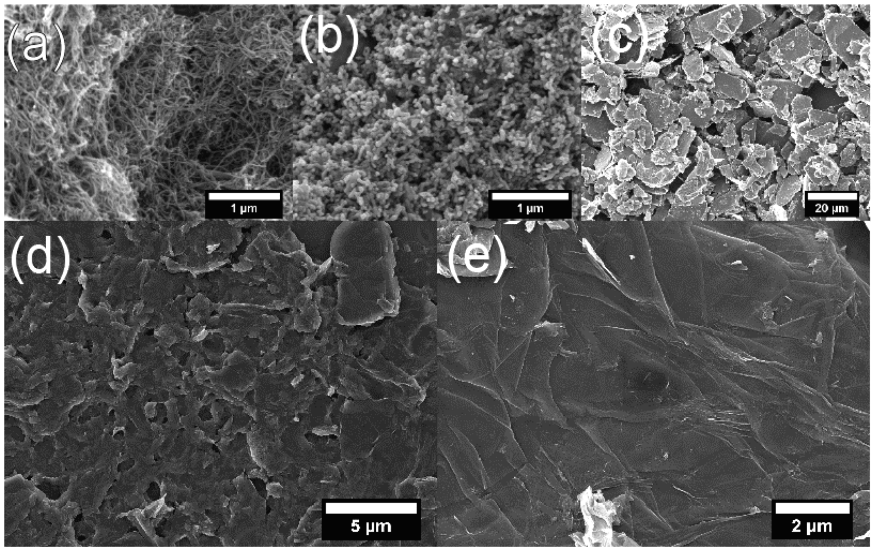

Figure 1. SEM images of (a) MWCNTs, (b) Co_3O_4 nanoparticles, (c) GP, (d) GO, and (e) graphene.

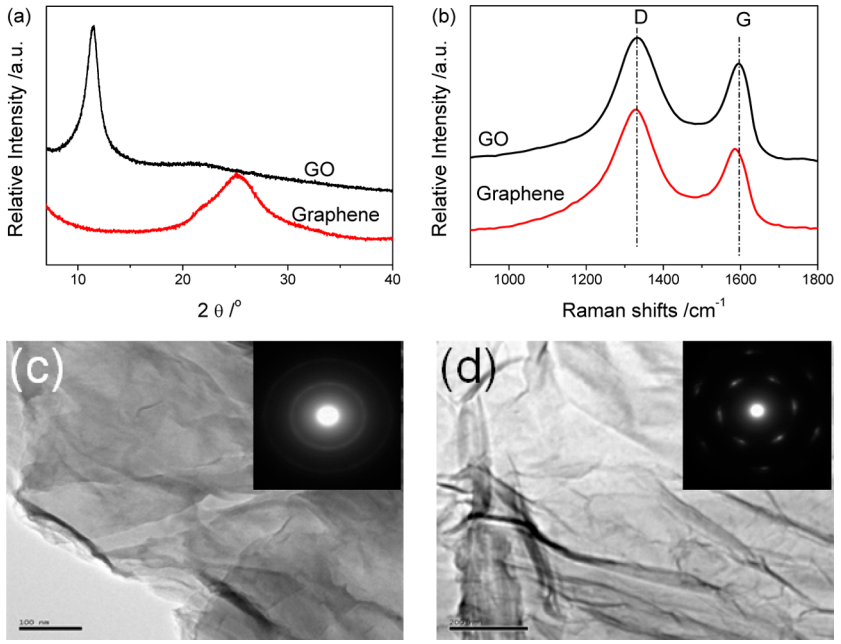

Figure 2. (a) XRD patterns of GO and graphene, (b) Raman spectra of GO and graphene, (c) TEM image of GO, and (d) TEM image of graphene. Inserts of c and d SAED patterns.

concentrated H_2SO_4 and $KMnO_4$, followed by H_2O_2 treatment. The obtained GO was separated by a centrifuge and washed by HNO_3/deionized water for several times. Lastly the GO was made from gels and dispersion by drying in air at 418 K and grinded finely. Detailed procedures can be found in a previous study.[30] Graphene was prepared by a hydrothermal process using a basic solution. Generally, 2 g of GO were mixed in 80 mL of ultrapure water and the mixture was stirred for 4 h. The suspension was then ultrasonically treated for 1 h. A concentrated ammonia solution (37 wt.%) was used to adjust the suspension to pH 10. The suspension was kept stirring overnight with a cover. Then, the mixture was transferred into a Teflon-lined autoclave (120 mL) and treated at 453 K for 18 h. The precipitate was washed by ultrapure water/ethanol for three times. After filtration, the chemically reduced graphene oxide was dried at 353 K. Cobalt oxide (Co_3O_4) was obtained by thermal decomposition of $Co(NO_3)_2$ at 773 K for 2 h. GP was commercially available natural graphite from Fluka. A multiwall carbon nanotube was received from Chengdu Organic Chemicals, China. An activated carbon was obtained from BDH Chemicals and was crushed into powder. All chemicals were used as received.

Sample Characterization. X-ray diffraction (XRD) patterns were obtained on a Bruker D8-Advanecd X-ray diffractometer with Cu Kα radiation (λ = 1.5418 Å), at accelerating voltage and current of 40 kV and 40 mA, respectively. Raman spectra were recorded on an ISA (Dilor) dispersive Raman spectrometer with argon ion 514 nm lasers. Fourier transform infrared spectra (FTIR) were acquired from a Bruker instrument using an ATR mode. Scanning electron microscopy (SEM) was performed on a Zeiss Neon 40EsB FIBSEM. Transmission electron microscopy (TEM) was operated on a JEOL 2011 TEM instrument. UV−visible adsorption spectra (UV−vis) were obtained from a Jasco V-570 UV−visible spectrometer.

Catalytic Degradation of Aqueous Contaminants. The catalytic oxidation of phenol, 2,4-dichlorophenol (DCP) and methylene blue (MB) was employed to probe the efficiency of activation of potassium peroxymonosulfate (using OXONE, $2KHSO_5{\cdot}KHSO_4{\cdot}K_2SO_4$ from Aldrich). The reactions were carried

dx.doi.org/10.1021/am301372d | ACS Appl. Mater. Interfaces 2012, 4, 5466−5471

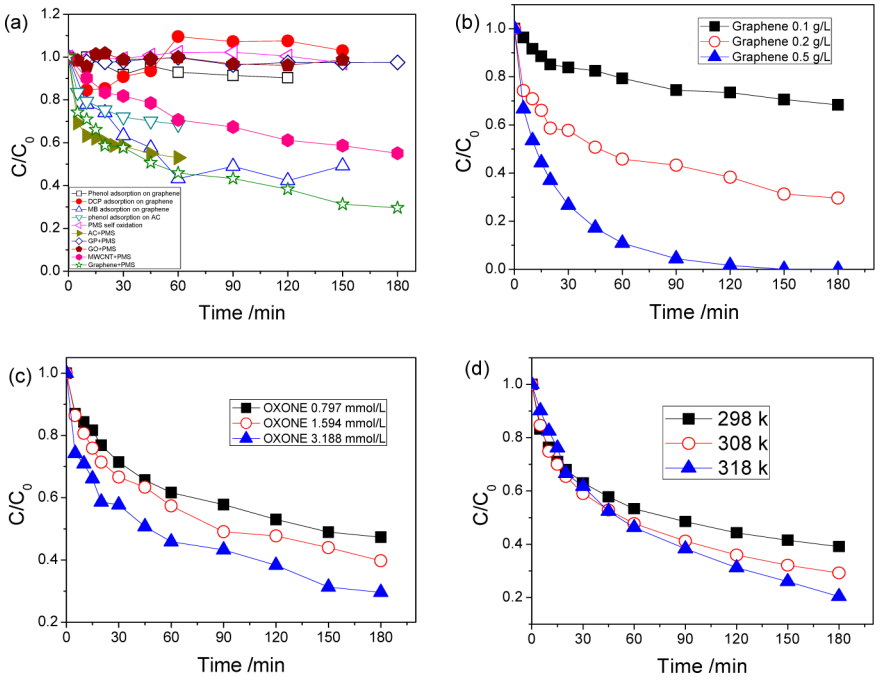

Figure 3. (a) Adsorption and carbon catalysis in activation of PMS for phenol oxidation [phenol = 2.125×10^{-4} mol/L; temperature = 298 K; catalyst = 0.2 g/L, and oxone = 3.188×10^{-3} mol/L], (b) effect of catalyst loadings, (c) effect of oxone amounts, and (d) effect of reaction temperatures.

out in a 500 mL reactor containing 2.125×10^{-4} mol/L of phenol solution (or 1.227×10^{-4} mol/L of DCP, or 3.135×10^{-5} mol/L MB). The reactor was attached to a stand and dipped into a water bath with a temperature controller (298, 308, or 318 K). A catalyst sample (0.1, 0.2, or 0.5 g/L) was first added to the solution and stirred for 10 min. Then OXONE (7.970×10^{-4}, 1.594×10^{-3} or 3.188×10^{-3} mol/L) was added to the mixture to start the reaction. The pH of reaction solution was not adjusted, and was about 6.5 at first, then decreased to 2−3 due to the influence from oxidation and oxidation processes. At each time interval, 1 mL of solution was withdrawn by a syringe and filtered by 0.45 μm Millpore film. The filtered solution was injected into a high performance liquid chromatograph (HPLC) vial which was filled with 0.5 mL of methanol as a quenching reagent. Phenol and DCP solutions were measured by a HPLC (Varian) with a C-18 column and MB was analyzed by a Jasco V-570 UV−visible spectrometer. Intermediates of phenol oxidation were analyzed by a HPLC using the same method with the flow rate down to 0.2 mL/min from 1.0 mL/min, and extending retention time to 25 min from 3 min. In the analysis of gas chromatograph−mass spectroscopy (GC-MS, Varian 3800/2200), 2.5 mL of methanol was added to 5 mL of reaction solution, and then 3 mL of dichloromethane (DCM) was added as an extractant. One microliter of extracted sample was injected into the GC-MS and was analyzed by a column with a temperature programmed method. In the stability test, the spent catalysts were recovered from the reaction mixture by filtration and washed thoroughly with DI water and dried at 353 K for repeated oxidation and characterization.

3. RESULTS

Characterization of Graphene. Figure 1 shows SEM (scanning electron microscopy) images of CNT, Co_3O_4, GP, GO, and graphene (G). The MWCNTs had an inner diameter of 2−5 nm, out diameter of 8−15 nm, and length of 10−30 μm. The prepared Co_3O_4 nanoparticles had a sphere-like morphology and aggregated with a particle size below 100 nm. The pristine GP had an irregular morphology at size of several tens of micrometers. After oxidation, randomly aggregated, wrinkled GO layers were produced. Such a morphology was generally observed at exfoliated GO.[35] Reduction of GO led to a more smooth surface, possibly due to the removal of oxygen-containing groups. Supporting Information Figure S1 shows the Fourier transform infrared spectra (FTIR) of GO and graphene, confirming the removal of surface groups by the successful reduction.

The crystalline structures of the various materials were analyzed by X-ray diffraction patterns (XRD). Figure 2 (a) shows XRD patterns of GO and graphene. XRD patterns of GP, MWCNT and Co_3O_4 can be found in Supporting Information Figure S2. On GO, a sharp peak at about 2θ = 11.4° corresponding to (002) reflection was observed, giving an interlayer spacing of 0.77 nm. The d spacing was larger than pristine graphite of 0.34 nm, indicating that C═C double bonds, ketone and enolic groups were introduced onto graphite (Supporting Information Figure S1). After reduction of GO, the peak at 11.4° disappeared and a broad peak at 25.1° emerged. Figure 2b presents Raman spectra of GO and G. Graphite lattice (G band) at 1596 cm^{-1} on GO and at 1585 cm^{-1} on graphene, respectively, was identified, against to 1580 cm^{-1} on GP. The shift of the G band to higher frequency on GO (1596 vs 1580 cm^{-1}) and a similar frequency on G to GP (1585 vs 1580 cm^{-1}) were consistent well with the results in Kudin's study.[36] Stronger graphite edges (D band) at 1330 cm^{-1} for GO and 1327 cm^{-1} for graphene were distinct from GP, indicating numerous defects were created. The I_D/I_G (band ratio of defect to graphite) of GO was determined to be 1.25, compared to 1.48 for graphene. The increased I_D/I_G of graphene was attributed to the reduction process. Transmission electron microscopy (TEM) images show that the GO (Figure 2c) and graphene (Figure 2d) might be of a multilayer structure, in relatively thick, stacked aggregates. Same as Yeh's observation,[27] selected-area electron diffraction (SAED) of GO showed diffraction rings that can be indexed to a hexagonal structure. In contrast, SAED of graphene showed spots

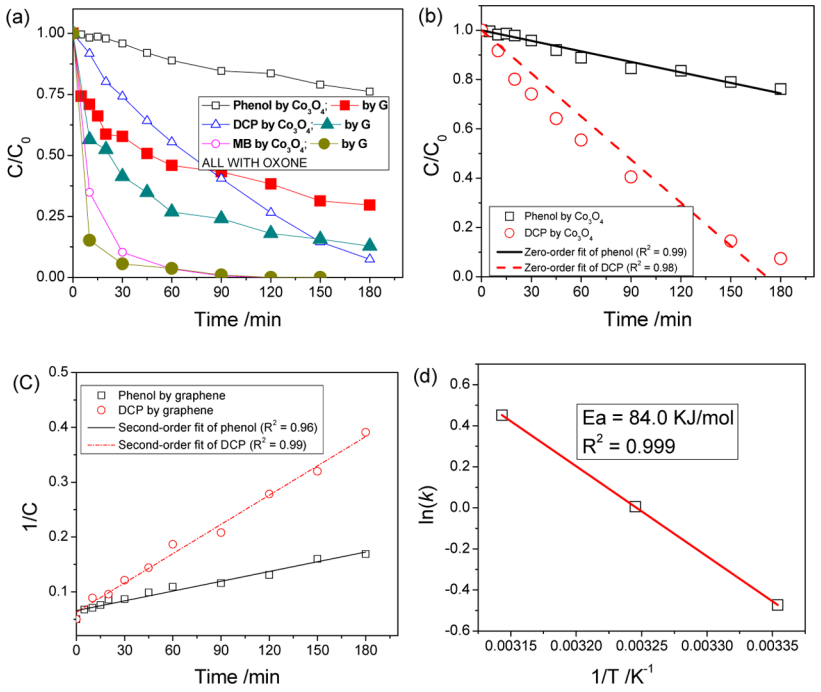

Figure 4. (a) Graphene-catalyzed oxidation of phenol, DCP, and MB with sulfate radicals in comparison to Co_3O_4, (b) zero-order kinetics of Co_3O_4, (c) second-order kinetics of graphene, and (d) Arrhenius plot of phenol degradation by graphene catalysis.

representing some of the graphite planes. The interspacing of GO at 0.44 nm suggested a notable oxidation level of sp^3 hybridization, while 0.42 nm for graphene was observed. After reduction, the optical property of GO was also changed (Supporting Information Figure S3).

The above characterization results strongly indicated that the GO was exfoliated and reduced to graphene with a high defective structure. The enriched defects, that is, zigzag edges, would play the role of active sites, alternative to metal active sites and provide a higher activity.

Catalytic Oxidation of Phenol. Figure 3a shows phenol removal at various conditions. Control experiments showed minimum adsorption of phenol (~10%) on graphene. Graphene hardly adsorbed DCP, but showed a high adsorption of MB. PMS was able to degrade little phenol by self-oxidation without the presence of a catalyst. The oxidation performance of GP and GO with PMS was similar to PMS self-oxidation, indicating that GP and GO are not able to activate PMS. The low activity of GP can be attributed to low density of defects, which determine the active sites of carbon catalyst.[37,38] GO has demonstrated its catalytic efficiency in photocatalysis,[27] oxidation and hydration reactions,[20] and dehydrative polymerization reactions.[26] The acidic nature of GO played a significant role in those reactions, yet, catalytic activation of PMS in this study favors on a basic surface.[16] The low activity of GO in activating PMS was then possibly due to the acidic surface. AC showed a high phenol removal, however, the phenol removal was mostly ascribed to adsorption: in 60 min 28% phenol removal by adsorption, 47% with addition of PMS.[5] Graphene was most effective among the carbon catalysts, providing 70.4% phenol removal in 3 h. In comparison, commercial MWCNT showed a phenol degradation of 45% at the same time.

Further kinetic studies were conducted to obtain insights into the graphene catalysis. Figure 3b shows that graphene usage would significantly influence phenol oxidation. Phenol removal at 90 min was 25.5, 56.7, and 95.6% for 0.1, 0.2, and 0.5 g/L graphene, respectively. Because of the minor adsorption on graphene, the significant changes in phenol removal were attributed to the enhanced active sites of graphene for catalysis. Figure 3c shows that increasing OXONE concentration from 7.970×10^{-4} to 3.188×10^{-3} mol/L slightly enhanced phenol degradation rate, and phenol degradation in 3 h was increased to 70.4% from 52.7%. The results implied that rate determining factor of phenol degradation was the quantity of active sites of graphene, confirming the graphene catalysis of the reaction, especially when considering the minor adsorption ability. The observation also showed the possibility for oxidation of organic pollutants with less disposal of sulfate (i.e., 3.188×10^{-3} mol/L). Unlike cobalt catalysis,[5,10,15] the reaction temperature imposed a less effect on phenol oxidation, as shown in Figure 3d. The weak temperature dependence of carrier mobility has been suggested to be the instinct feature of graphene.[39,40] This might be part of the reason that temperature can only slightly affect the catalytic reaction.

Comparison to Transition Metal-Based Catalyst. We further evaluated the catalytic activity of graphene in oxidation of phenol, DCP and MB in comparison to a typical cobalt oxide, Co_3O_4. It was found that in all three systems, graphene showed a promising efficiency in activating PMS for oxidation, as shown in Figure 4a. In phenol oxidation, graphene removed 70.4% of phenol at 180 min, compared to 23.9% on Co_3O_4 nanoparticles. In DCP oxidation, graphene was able to degrade 76.0% of DCP at 90 min, while that of Co_3O_4 was 59.5%. For MB degradation, decoloration of MB on graphene was 84.8% at 10 min, compared to 22.0% adsorption on graphene and 65.2% on Co_3O_4. The results strongly suggested that graphene catalysis can be a powerful approach for environmental catalysis. Cobalt catalysis was observed as a zero-order kinetics, whereas graphene catalysis was fitted better as a second-order kinetics, as shown in Figure 4b and c. Previous studies showed that Co ion exchanged zeolite (Co/ZSM-5)[15] and Co/SiO_2[41] followed a zero-order kinetics in phenol degradation with

dx.doi.org/10.1021/am301372d | ACS Appl. Mater. Interfaces 2012, 4, 5466−5471

sulfate radicals, while Co/AC followed a first-order kinetics.[5] For kinetics on carbon catalysis, Zhang et al.[21] observed 0.5−0.6 reaction order in CNT catalyzed oxidative dehydrogenation (ODH) of ethylbenzene. The detailed understanding of the fate of active sites of graphene and the instant concentration of radicals were remained unknown, thus it was difficult to justify the difference between graphene catalysis and cobalt catalysis. Figure 4d shows the estimation of activation energy of graphene catalyzed oxidation of phenol with sulfate radicals. The activation energy was estimated to be 84.0 kJ/mol, with a high regression coefficient of 0.999. The activation energy of graphene was higher than those of supported cobalt catalysts, e.g., 61.7−75.5 kJ/mol on Co/SiO_2,[41] 67.4 kJ/mol on Co/SBA-15,[38] 69.7 kJ/mol on Co/ZSM-5,[15] and 59.7 kJ/mol on Co/AC.[5] In general, carbon catalysts have a large activation energy. In a recent study, an activation energy of 125 ± 3 kJ/mol was observed in the hydrothermal decarboxylation of palmitic acid by activated carbon.[42] The activation energy in ODH reactions by a CNT was 68−75 kJ/mol.[21]

4. DISCUSSION

The stability of graphene in repeated use was shown in Supporting Information Figure S4. On the basis of the phenol removal rate at 120 min, 56.5% of activity was achieved at the second run and 25.5% at the third use. Such a performance was comparable to or better than some supported cobalt catalysts.[10,41] The morphology, crystalline phase and defective structure of used catalyst were analyzed, seen in Supporting Information Figure S5. It was found that no significant changes were observed before and after the catalytic reactions, indicating that the deactivation might be due to the coverage of intermediates. Raman spectra showed extra peaks due to the produced intermediates. The intermediates from graphene catalysis and Co catalysis were analyzed based on HPLC spectra (Supporting Information Figure S6a). We applied a variety of pure chemicals to be checked by HPLC and concluded that three main intermediates, 4-hydroxybenzonic acid, p-benzoquinone, and 1,2-dihydroxybenzene were present in the reaction solutions of the two systems. Supporting Information Figure S6b further suggests that both phenol and intermediates would be decreased with increasing reaction time. It was found that same main intermediates were present in both graphene- and cobalt-systems, suggesting similar phenol decomposition pathways. Very weak peaks were observed in PMS self-oxidation system, confirming the results in Figure 3a that PMS only oxidizes very little amount of phenol. The reaction solutions of graphene-PMS at reaction time 0 and 10 min were further analyzed by GC-MS, with a comparison to the pure extractant (Supporting Information Figure S7). The emerging intermediates were indicatively shown in Supporting Information Table 1S. The produced intermediates strongly suggested that phenol removal was due to catalytic degradation, not by adsorption.

In the system of cobalt-based catalyst, the nature of heterogeneous catalysis was the formation of surface species of $CoOH^+$ on Co_3O_4 ($CoO{\cdot}Co_2O_3$). The activation reactions were listed as below.

$$CoOH^+ + HSO_5^- \rightarrow CoO^+ + SO_4^{\bullet -} + H_2O \quad (1)$$

$$CoO^+ + 2H^+ \rightarrow Co^{3+} + H_2O \quad (2)$$

In this hypothesis, $CoO{\cdot}Co_2O_3$ facilitates a redox cycle for sulfate radical generation. Heterogeneous carbon catalysis is free of polyvalent metal sites with complex electronic and spin culture, giving rise to a facile and in-depth theoretical analysis. The activation of PMS by graphene in this study would be more similar to those in ODH (oxidative dehydrogenation) and DH (dehydrogenation) reactions, which utilized Lewis basic sites of nanocarbons.[21,23,24] The hydrothermal reduction of GO was able to tune the surface acidity/alkalinity by removal of oxygen-containing groups. The activity of graphene in activation of PMS was then improved by altering surface acidity of GO to alkaline by ammonia solution.

Furthermore, the active sites of graphene in activation of PMS would be the zigzag edges. For a basal plane in perfect graphene, sp^2 carbon atoms are located in a hexagonal cell as a π-conjugated system. Edge defects and curvature at stacked graphene layers produce nonsix-membered carbon rings. Depending on the orientation that C−C σ bonds are broken, two types of edges, zigzag and armchair are produced. The localized state at zigzag edge makes their π electrons not to be confined by the edge carbons, therefore higher chemical activity is expected.[37,38] Chemically reduced graphene oxide would retain little amount of oxygen-containing groups at zigzag edges, and the remaining groups have a higher intrinsic activity than those terminating the flat (001) surface.[25] The oxygen functional surface species, such as ketonic (C═O) groups, are rich in electrons and thus have a great potential to coordinate a redox process.[23] The graphene catalysis would be carried out following the reactions shown in eqs 3 and 4, with donated electrons from graphene to PMS for producing $SO_4^{\bullet -}$.

$$HSO_5^- + e^- \rightarrow SO_4^{\bullet -} + HO^- \quad (3)$$

$$HSO_5^- + h^+ \rightarrow SO_5^{\bullet -} + H^+ \quad (4)$$

Scheme 1 shows the activation of PMS by graphene and the consequent phenol oxidation. PMS (HSO_5^-) is able to activated by graphene to produce two kinds of sulfate radicals,

Scheme 1. Graphene Activation of PMS and Its Probing Reaction

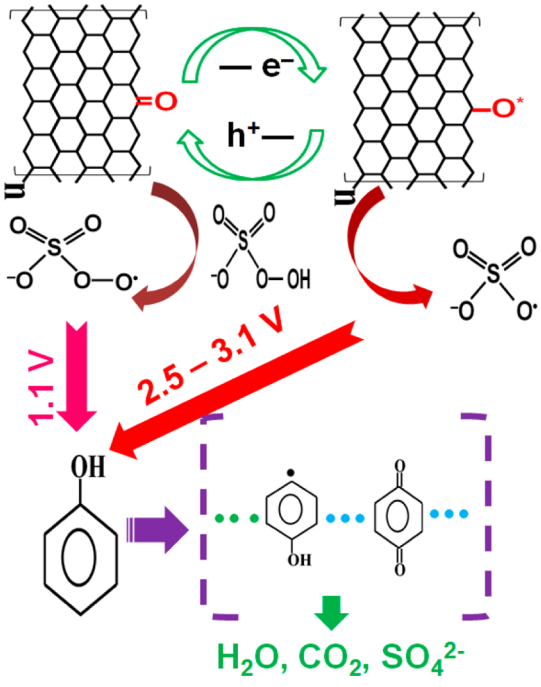

dx.doi.org/10.1021/am301372d | ACS Appl. Mater. Interfaces 2012, 4, 5466−5471

$SO_4^{\bullet-}$ and $SO_5^{\bullet-}$. The former radical has a higher oxidative potential (2.5−3.1 V) and will play key role in degradation of phenol. As confirmed by HPLC and GC-MS, a variety of intermediates will be produced. At last, the intermediates will be finally decomposed to CO_2 and H_2O. This mechanism is supported by following observations: (a) activity of various carbons in an order of graphene > MWCNT > GP > GO, corresponding to their graphite defects density, (b) activity closely related to the catalyst loading, (c) weak temperature dependence representing graphene carriers character,[39,40] and (d) analogues to the similar catalysis applying to nanocarbons.[20,21,25,43]

5. CONCLUSION

It is concluded that structure defective graphene was able to effectively activate PMS to produce active sulfate radicals. In the probing experiments, we demonstrated that the produced radicals were competent in decomposition of phenol, chlorophenols and dyes. The activity of graphene was not only higher than other carbons, such as GP, AC, MWCNT, and GO, but superior to popular transition metal oxides. Such catalysis is expected not only to be applied in environmental catalysis, but to be extended to other potential catalytic processes.

■ ASSOCIATED CONTENT

Ⓢ Supporting Information

Additional XRD patterns, FTIR spectra, UV−vis absorption spectra, stability tests, characterization of catalysts before and after use (XRD, SEM, and Raman), HPLC spectra, and GC-MS spectra. This material is available free of charge via the Internet at http://pubs.acs.org.

■ AUTHOR INFORMATION

Corresponding Author

*E-mail: shaobin.wang@curtin.edu.au (S.W.); h.sun@curtin.edu.au (H.S.).

Notes

The authors declare no competing financial interest.

■ REFERENCES

(1) Cantu, M.; Lopez-Salinas, E.; Valente, J. S. *Environ. Sci. Technol.* **2005**, *39*, 9715−9720.
(2) Feng, X. B.; Hall, W. K. *J. Catal.* **1997**, *166*, 368−376.
(3) Patel, A.; Shukla, P.; Rufford, T.; Wang, S. B.; Chen, J. L.; Rudolph, V.; Zhu, Z. H. *Appl. Catal. A: Gen.* **2011**, *409*, 55−65.
(4) Sun, H. Q.; Ullah, R.; Chong, S. H.; Ang, H. M.; Tade, M. O.; Wang, S. B. *Appl. Catal. B: Environ.* **2011**, *108*, 127−133.
(5) Shukla, P. R.; Wang, S. B.; Sun, H. Q.; Ang, H. M.; Tade, M. *Appl. Catal. B: Environ.* **2010**, *100*, 529−534.
(6) Sun, H. Q.; Bai, Y.; Liu, H. J.; Jin, W. Q.; Xu, N. P.; Chen, G. J.; Xu, B. Q. *J. Phys. Chem. C* **2008**, *112*, 13304−13309.
(7) Gonzalez-Velasco, J. R.; Aranzabal, A.; Gutierrez-Ortiz, J. I.; Lopez-Fonseca, R.; Gutierrez-Ortiz, M. A. *Appl. Catal. B: Environ.* **1998**, *19*, 189−197.
(8) Scire, S.; Minico, S.; Crisafulli, C.; Satriano, C.; Pistone, A. *Appl. Catal. B: Environ.* **2003**, *40*, 43−49.
(9) Sun, W. T.; Yu, Y.; Pan, H. Y.; Gao, X. F.; Chen, Q.; Peng, L. M. *J. Am. Chem. Soc.* **2008**, *130*, 1124−1125.
(10) Shukla, P.; Sun, H. Q.; Wang, S. B.; Ang, H. M.; Tade, M. O. *Catal. Today.* **2011**, *175*, 380−385.
(11) Anipsitakis, G. P.; Dionysiou, D. D. *Environ. Sci. Technol.* **2004**, *38*, 3705−3712.
(12) Anipsitakis, G. P.; Dionysiou, D. D.; Gonzalez, M. A. *Environ. Sci. Technol.* **2006**, *40*, 1000−1007.
(13) Ling, S. K.; Wang, S. B.; Peng, Y. L. *J. Hazard. Mater.* **2010**, *178*, 385−389.
(14) Anipsitakis, G. P.; Stathatos, E.; Dionysiou, D. D. *J. Phys. Chem. B* **2005**, *109*, 13052−13055.
(15) Shukla, P.; Wang, S. B.; Singh, K.; Ang, H. M.; Tade, M. O. *Appl. Catal. B: Environ.* **2010**, *99*, 163−169.
(16) Zhang, W.; Tay, H. L.; Lim, S. S.; Wang, Y. S.; Zhong, Z. Y.; Xu, R. *Appl. Catal. B: Environ.* **2010**, *95*, 93−99.
(17) Su, D. S.; Zhang, J.; Frank, B.; Thomas, A.; Wang, X. C.; Paraknowitsch, J.; Schlogl, R. *ChemSusChem* **2010**, *3*, 169−180.
(18) Dreyer, D. R.; Bielawski, C. W. *Chem. Sci.* **2011**, *2*, 1233−1240.
(19) Pyun, J. *Angew. Chem. Inter. Ed.* **2011**, *50*, 46−48.
(20) Dreyer, D. R.; Jia, H. P.; Bielawski, C. W. *Angew. Chem. Int. Ed.* **2010**, *49*, 6813−6816.
(21) Zhang, J.; Su, D. S.; Zhang, A. H.; Wang, D.; Schlogl, R.; Hebert, C. *Angew. Chem. Int. Ed.* **2007**, *46*, 7319−7323.
(22) Zhang, J.; Liu, X.; Blume, R.; Zhang, A. H.; Schlogl, R.; Su, D. S. *Science* **2008**, *322*, 73−77.
(23) Frank, B.; Zhang, J.; Blume, R.; Schlogl, R.; Su, D. S. *Angew. Chem. Int. Ed.* **2009**, *48*, 6913−6917.
(24) Zhang, J. A.; Su, D. S.; Blume, R.; Schlogl, R.; Wang, R.; Yang, X. G.; Gajovic, A. *Angew. Chem. Int. Ed.* **2010**, *49*, 8640−8644.
(25) Frank, B.; Blume, R.; Rinaldi, A.; Trunschke, A.; Schlögl, R. *Angew. Chem. Int. Ed.* **2011**, *50*, 10226−10230.
(26) Dreyer, D. R.; Jarvis, K. A.; Ferreira, P. J.; Bielawski, C. W. *Macromolecules* **2011**, *44*, 7659−7667.
(27) Yeh, T. F.; Syu, J. M.; Cheng, C.; Chang, T. H.; Teng, H. S. *Adv. Funct. Mater.* **2010**, *20*, 2255−2262.
(28) Zhang, L. L.; Xiong, Z. G.; Zhao, X. S. *ACS Nano* **2010**, *4*, 7030−7036.
(29) Jang, D. M.; Myung, Y.; Im, H. S.; Seo, Y. S.; Cho, Y. J.; Lee, C. W.; Park, J.; Jee, A. Y.; Lee, M. *Chem. Commun.* **2012**, *48*, 696−698.
(30) Bradder, P.; Ling, S. K.; Wang, S. B.; Liu, S. M. *J. Chem. Eng. Data* **2011**, *56*, 138−141.
(31) Ramesha, G. K.; Kumara, A. V.; Muralidhara, H. B.; Sampath, S. *J. Colloid Interface Sci.* **2011**, *361*, 270−277.
(32) Zhao, G. X.; Li, J. X.; Ren, X. M.; Chen, C. L.; Wang, X. K. *Environ. Sci. Technol.* **2011**, *45*, 10454−10462.
(33) Liao, G. Z.; Chen, S.; Quan, X.; Yu, H. T.; Zhao, H. M. *J. Mater. Chem.* **2012**, *22*, 2721−2726.
(34) Hummers, W. S.; Offeman, R. E. *J. Am. Chem. Soc.* **1958**, *80*, 1339−1339.
(35) Zhou, Y.; Bao, Q. L.; Tang, L. A. L.; Zhong, Y. L.; Loh, K. P. *Chem. Mater.* **2009**, *21*, 2950−2956.
(36) Kudin, K. N.; Ozbas, B.; Schniepp, H. C.; Prud'homme, R. K.; Aksay, I. A.; Car, R. *Nano Lett.* **2008**, *8*, 36−41.
(37) Lee, G.; Cho, K. *Phys. Rev. B* **2009**, *79*, 165440.
(38) Jiang, D. E.; Sumpter, B. G.; Dai, S. *J. Chem. Phys.* **2007**, *126*, 134701.
(39) Novoselov, K. S.; Geim, A. K.; Morozov, S. V.; Jiang, D.; Katsnelson, M. I.; Grigorieva, I. V.; Dubonos, S. V.; Firsov, A. A. *Nature* **2005**, *438*, 197−200.
(40) Geim, A. K.; Novoselov, K. S. *Nat. Mater.* **2007**, *6*, 183−191.
(41) Shukla, P.; Sun, H. Q.; Wang, S. B.; Ang, H. M.; Tade, M. O. *Sep. Purif. Technol.* **2011**, *77*, 230−236.
(42) Fu, J.; Shi, F.; Thompson, L. T.; Lu, X. Y.; Savage, P. E. *ACS Catal.* **2011**, *1*, 227−231.
(43) Gao, Y. J.; Ma, D.; Wang, C. L.; Guan, J.; Bao, X. H. *Chem. Commun.* **2011**, *47*, 2432−2434.